On-Orbit Damage Assessment for Large Space Structures

Jay-Chung Chen* and John A. Garba†
Jet Propulsion Laboratory, California Institute of Technology, Pasadena, California

The need to monitor the dynamic characteristics of large structural systems for purposes of assessing the potential degradation of structural properties has been established. This paper develops a theory for assessing the occurrence, location, and extent of potential damage using on-orbit response measurements. Feasibility of the method is demonstrated using a simple structural system as an example.

Introduction

MOST load-carrying structural systems such as aircraft, spacecraft, high-rise buildings, and offshore platforms continuously accumulate damage in their service environment. In order to assure safety, it is most desirable that this damage be monitored to assess its occurrence, location, and extent.

Large space structures in Earth orbit or on interplanetary missions are apt to suffer structural damage over their service time caused by such adverse events as docking, impact by foreign objects, and other hostile actions, and from environmental effects due to long exposure to space such as thermal vacuum, radiation, and ultraviolet light. Damage that is not detected and not corrected may potentially cause more damage and eventually catastrophic structural failure. Therefore, a methodology for monitoring the structural integrity in order to rapidly detect the occurrence and identify the location of damage will be instrumental in assuring the safety of the structural system. In particular, such detection can permit real-time corrective action or a change in operational procedures to minimize the possibility of causing further damage.

As configurations of space structures become larger and more complex, the use of exotic materials will become more common, and the functional requirements of the structural systems will become complex and critical. Hence, a rapid and remote structural damage detection capability will be more essential. In the case of the Space Station, one common attribute of all proposed configurations is the complexity of the structural system. A typical configuration consists of many bays connected in a complicated manner, each of which is a three-dimensional structure. Components include antennas, solar arrays, docking structures, fluid containers, and many other complex systems. Should one or more structural components incur damage in such a large system, it may be virtually impossible to detect the presence of the damage, let alone locate it and quantify the extent. For major structural failures such as rupture of major truss member, visual inspection may be sufficient to locate and assess the damage. However, it is very difficult to observe visually any damage due to material degradation, since the surface appearance most likely will remain unchanged. It is, therefore, necessary that for damage detection and assessment the characteristics of the structure, which include the load-carrying capability as its inherent property, be monitored.

It becomes clear that continuous monitoring of structural integrity and the detection and assessment of damage and its subsequent compensation, repair, and control are important considerations for large flexible space structures. The ultimate future requirement will be a remote data acquisition system with rapid onboard analysis for almost real-time assessment. The present study will focus on the feasibility of such a methodology that will provide a damage assessment capability for large space structures.

Approach

Techniques of using experimentally measured data for determining the parameters in the equations of motion of a system commonly are called system identification. A typical procedure involves the modal test of the structural system during which the responses due to external excitations are measured. From the response data, the dynamic characteristics of the system such as the natural frequencies and mode shapes can be determined directly or through data processing techniques, depending on the test method employed. Because the natural frequencies and mode shapes of a structural system are functions of the system parameters such as the mass and stiffness, these system parameters may be identified by comparing those determined by test to those dynamic characteristics predicted from the mathematical model. Based on this concept, attempts have recently been made to develop techniques for using vibration measurements to evaluate the structural integrity of offshore oil and gas platforms.[1-3] Because of the adverse conditions in acquiring these measurements, the high redundancy of the structural system, and the lack of sufficient instrumentation, the methodology of detection of structural failures did not become mature. The technology is not being implemented by the platform industry at the present time. On the other hand, in the aerospace industry modal tests are performed on extensively instrumented spacecraft using precisely controlled excitations for determining natural frequencies, mode shapes, and damping. Here, the objective is to verify the mathematical model to be used in loads analysis by comparing the dynamic characteristics obtained by a test to those predicted by the analytical model. The differences between the test and analysis results are then used to modify the mathematical model so that the model accurately predicts the test results.[4-8] Furthermore, it is very likely that on-orbit modal testing is necessary for the large space structures because of the adaptive control requirement. These modal test results can be made available for the purpose of on-orbit damage assessment.

In the present study, the investigation will be centered around developing methodology to use the test-measured data or test-determined dynamic characteristics not to verify the

Received Feb. 20, 1987; presented as Paper 87-8070 at the AIAA 28th Structures, Structural Dynamics, and Materials Conference, Monterey, CA, April 6-8, 1987; revision received Dec. 8, 1987.

*Member of Technical Staff, Applied Technologies Section. Member AIAA.

†Supervisor, Structures and Dynamics Research Group. Member AIAA.

mathematical model but rather to identify the damage of the structure in terms of its location and the extent, i.e., the reduction of stiffness or load-carrying capability.

Theoretical Development

The fundamental questions for damage assessment are whether it is feasible to identify the occurrence, location, and extent of the damage from given measured structural dynamic characteristics. Therefore, the relationship between the physical parameters, such as the mass and stiffness, and the dynamic characteristics, such as the eigenvalues and eigenvectors or natural frequency and mode shape, must be established. The governing equations for the structural dynamic system in finite-element representation can be written as

$$[M]\{\ddot{x}\} + [C]\{\dot{x}\} + [K]\{x\} = \{f(t)\} \tag{1}$$

where the matrices $[M]$, $[C]$, and $[K]$ represent the discretized mass and inertia, damping, and stiffness distribution; $\{\ddot{x}\}$, $\{\dot{x}\}$, and $\{x\}$ are the acceleration, velocity, and displacement vectors of the degrees of freedom being modeled, and $\{f(t)\}$ is the external forcing function vector. The homogeneous solutions to Eq. (1) are the eigenvalues and the eigenvectors. For simplicity, the damping terms will be ignored at the present time, thus

$$[M]\{\ddot{x}\} + [K]\{x\} = 0 \tag{2}$$

Let

$$\{x\} = \{\phi\}_i \sin\omega_i t \tag{3}$$

where ω_i is the ith eigenvalue, and $\{\phi\}_i$ is the corresponding eigenvector. Upon substitution into Eq. (2), the relationship between the physical parameters $[M]$ and $[K]$ and the dynamic characteristics ω_i and $\{\phi\}_i$ can be established as

$$[K]\{\phi\}_i - \omega_i^2[M]\{\phi\}_i = 0 \tag{4}$$

It is clear that values of ω_i and $\{\phi\}_i$ are functions of the mass $[M]$ and $[K]$ of the system. In other words, any changes in $[M]$ and $[K]$ due to the loss of mass or loss of stiffness of certain parts of the structural system will be reflected in its natural frequency and mode shape measurements. A discovery of a deviation of the measured natural frequency and mode shape with respect to those previously measured when the system was in an undamaged condition indicates the occurrence of damage. Certain changes in the physical parameters will effect certain modes but not others. The occurrence of damage will not be detected if only those modes that are not affected by the changes are measured. To establish damage assessment, a wide range of measurements should be made to ensure the inclusion of the effected modes.

Next, the feasibility of locating the damage will be investigated. First, it will be postulated that the mass distribution of the system $[M]$ remains either unchanged or is changed by only a known quantity. This is a reasonable assumption because most structural damage for the large space structures will result in stiffness losses instead of complete separation or breakage with a loss of mass. Also, for certain large space structures such as the Space Station, the major contribution to the mass matrix comes from nonload-carrying components such as instrument packages, fluid containers, and power generation units. These weights can be accurately estimated. Multiplying Eq. (4) by a diagonal matrix $\lceil\phi\rfloor_i$, one obtains the following:

$$\lceil\phi\rfloor_i [K]\{\phi\}_i = \omega_i^2 \lceil\phi\rfloor_i [M]\{\phi\}_i \tag{5}$$

Without loss of generality, the mass matrix $[M]$ will be assumed to be diagonal; then the right-hand side of Eq. (5) will be

$$\omega_i^2 \lceil\phi\rfloor_i \lceil M_{ji}\rfloor \{\phi\}_{ji} = \omega_i^2 \left\{M_{jj}\phi_{ji}^2\right\} \tag{6}$$

The expression on the right-hand side of Eq. (6) clearly represents kinetic energy. Equations (5) and (6) indicate that the kinetic energy distribution at each degree of freedom for the ith mode is equal to the potential energy distribution. The potential energy distribution is a function only of the stiffness matrix and the modal displacements. For localized damage, the mode shape should be similar to or only slightly deviated from that of the undamaged system. Hence, the potential energy distribution will be similar except for those degrees of freedom associated with the damaged component. The location of the damage can be found by identifying those degrees of freedom whose kinetic energies are different from those of the undamaged system. Since the correct stiffness matrix for the damaged system is unknown, the kinetic energy distribution can be used for this purpose instead. It should be noted from Eq. (6) that the kinetic energy distribution is a function of the mass matrix and the modal displacement. The frequency does not effect the relative distribution among each degree of freedom. Unlike the detection of damage occurrence, frequency measurement alone is not sufficient, and mode shape measurements are required for locating the damage.

The next task is to quantify the extent of the damage. For this purpose, Eq. (4) will be used in which the stiffness and mass matrices and the eigenvalue and eigenvector all are assumed to be part of the damaged system. The stiffness matrix will be decomposed into

$$[K] = [K_0] + [\Delta K] \tag{7}$$

where $[K_0]$ is the stiffness matrix for the undamaged system, and $[\Delta K]$ is the perturbation due to the structural damage.

Substituting Eq. (7) into Eq. (4), one obtains

$$[\Delta K]\{\phi\}_i = \left(\omega_i^2[M] - [K_0]\right)\{\phi\}_i \tag{8}$$

The right-hand side of Eq. (8) and $\{\phi\}_i$ are known quantities. The unknowns are the elements in the $[\Delta K]$ matrix, which will be denoted as $[\Delta k_{ij}]$. Let

$$[\Delta K]\{\phi\}_i = [\Delta k_{ij}]\{\phi\}_i = [C]_i\{\Delta k_{ij}\} \tag{9}$$

where $[C]_i$ is defined as the connectivity matrix for the ith mode. The elements in the connectivity matrix are a function of the elements from the ith modal displacement $\{\phi\}_i$. Substituting Eq. (9) into Eq. (8), one obtains

$$[C]_i\{\Delta k_{ij}\} = \{y\}_i \tag{10}$$

where

$$\{y\}_i = \left(\omega_i^2[M] - [K_0]\right)\{\phi\}_i \tag{11}$$

It should be noted that the dimensions of the vectors $\{y\}_i$ and $\{\Delta k_{ij}\}$ are different. The dimension of $\{y\}_i$ is equal to the number of the degree of freedom of the system, and the dimension of $\{\Delta k_{ij}\}$ will be equal to the number of independent elements in the stiffness matrix. Although the stiffness matrix is highly banded, the number of independent elements is usually larger than the number of the degrees of freedom of the system. In other words, Eq. (10) is a set of algebraic equations in which there are more unknowns, the Δk_{ij}, than there are equations. In principle, there are an infinite number of $\{\Delta k_{ij}\}$ vectors that will satisfy Eq. (10).

Equation (10) is obtained by using measurements from a single mode, namely, the ith mode. For using multiple modes, the governing equations can be written as

$$\begin{bmatrix} [C]_1 \\ [C]_2 \\ \vdots \\ [C]_n \end{bmatrix} \{\Delta k_{ij}\} = \begin{Bmatrix} \{y\}_1 \\ \{y\}_2 \\ \vdots \\ \{y\}_n \end{Bmatrix} \tag{12}$$

The number of unknowns in Eq. (12) remains the same as that of Eq. (10); however, the number of equations has been increased. It is possible that the number of equations becomes larger than the number of unknowns. In principle, a solution to Eq. (12) might not exist. The procedure for solving for $\{\Delta k_{ij}\}$ in either Eq. (10) or (12) will be discussed next. The equations to be solved can be written as

$$\begin{aligned} &\text{Dimension} = (N \times M)\ (M \times 1) \quad (N \times 1) \\ &[C] \quad \{\Delta k_{ij}\} = \{Y\} \end{aligned} \tag{13}$$

where N is the number of equations, and M is the number of Δk_{ij}, the unknown. The solution procedure will be outlined for three different cases.

Case 1, $M > N$

If the number of unknowns is greater than the number of equations, Eq. (13) yields an infinite number of solutions. Because of the nature of the problem, namely, to seek the changes in the stiffness of structural elements as represented by the quantities Δk_{ij}, it is reasonable to postulate that the optimal solution is the one with the smallest Euclidian norm. Thus, the solution procedure becomes a constrained minimization subject to Eq. (13). The procedure can be formulated as

$$E = \tfrac{1}{2}\|\Delta k_{ij}\| + \{\lambda\}^T(\{Y\} - [C]\{\Delta k_{ij}\}) \tag{14}$$

where

$$\left.\begin{aligned} \|\Delta k_{ij}\| &= \{\Delta k_{ij}\}^T\{\Delta k_{ij}\}\ \text{Euclidian norm} \\ \{\lambda\} &= \text{vector of Lagrange multipliers} \end{aligned}\right\} \tag{15}$$

$$\frac{\partial E}{\partial(\Delta k_{ij})} = \{\Delta k_{ij}\} - [C]^T\{\lambda\} = 0 \tag{16}$$

$$\left\{\frac{\partial E}{\partial \lambda}\right\} = \{Y\} - [C]\{\Delta k_{ij}\} = 0 \tag{17}$$

From Eq. (16), one obtains

$$\{\Delta k_{ij}\} = [C]^T\{\lambda\} \tag{18}$$

Substituting Eq. (18) into Eq. (17), one obtains

$$\{Y\} = [C][C]^T\{\lambda\} \tag{19}$$

$$\{\lambda\} = \left([C][C]^T\right)^{-1}\{Y\} \tag{20}$$

From Eqs. (20) and (18), the optimal solution becomes

$$\{\Delta k_{ij}\} = [C]^T\left([C][C]^T\right)^{-1}\{Y\} \tag{21}$$

Case 2, $N > M$

If the number of equations is greater than the number of unknowns, no exact solution exists. Therefore, one may look for an approximate solution in which the Euclidian norm of the error is minimized. Let

$$\{\epsilon\} = \{Y\} - [C]\{\Delta k_{ij}\} \tag{22}$$

$$\begin{aligned} \|\epsilon^2\| &= \{\epsilon\}^T\{\epsilon\} \\ &= \left(\{Y\} - [C]\{\Delta k_{ij}\}\right)^T\left(\{Y\} - [C]\{\Delta k_{ij}\}\right) \end{aligned} \tag{23}$$

The minimization procedure will provide

$$\left\{\frac{\partial\|\epsilon^2\|}{\partial(\Delta k_{ij})}\right\} = -2[C]^T\{Y\} + 2[C]^T[C]\{\Delta k_{ij}\} = 0 \tag{24}$$

Thus

$$\{\Delta k_{ij}\} = \left([C]^T[C]\right)^{-1}[C]^T\{Y\} \tag{25}$$

Case 3, $N = M$

When the number of equations and the number of unknowns are equal, an exact solution can be obtained; thus

$$\{\Delta k_{ij}\} = [C]^{-1}\{Y\} \tag{26}$$

It should be noted that the norm minimization of $\|\Delta k_{ij}\|$ and $\|\epsilon^2\|$ of Eqs. (14) and (23), respectively, can be performed for weighted norms. The purpose of the weighted norm is to choose a relative emphasis of the components of the vector norm being minimized. The weighting matrix $[Q]$ should be compatible and positive definite. Equations (14) and (23), respectively, can be written as

$$E = \tfrac{1}{2}\{\Delta k_{ij}\}^T[Q]\{\Delta k_{ij}\} + \{\lambda\}(\{Y\} - [C]\{\Delta k_{ij}\}) \tag{27}$$

$$\begin{aligned} \|\epsilon^2\| &= \{\epsilon\}^T[Q]\{\epsilon\} = \left(\{Y\} - [C]\{\Delta k_{ij}\}\right)^T[Q](\{Y\} \\ &\quad -[C]\{\Delta k_{ij}\}) \end{aligned} \tag{28}$$

The corresponding solutions for Cases 1 and 2 will be

$$\{\Delta k_{ij}\} = [Q]^{-1}[C]^T\left([C][Q]^{-1}[C]^T\right)^{-1}\{Y\} \tag{29}$$

$$\{\Delta k_{ij}\} = \left([C]^T[Q][C]\right)^{-1}[C]^T[Q]\{Y\} \tag{30}$$

Thus, a consistent and unified approach for estimating the structural damage has been derived. The next task is to demonstrate the procedure outlined above by using an example.

Illustrative Example

A simple example will be used for the purpose of illustrating the proposed approach for the assessment of structural damage. Figure 1 shows a three-degree-of-freedom system to be used as an example for both the undamaged and damaged configurations. The "damage" is assumed to be the complete breakage of the spring k_4. The mass and stiffness matrices for the undamaged configuration are

$$[M] = \begin{bmatrix} 6 & 0 & 0 \\ 0 & 4 & 0 \\ 0 & 0 & 4 \end{bmatrix} \qquad [K] = \begin{bmatrix} 6 & -3 & 0 \\ -3 & 6 & -3 \\ 0 & -3 & 4 \end{bmatrix} \tag{31}$$

The mass matrix for damaged system is the same as that of the undamaged system, but the stiffness matrix will be assumed unknown. The eigenvalues and eigenvectors of both systems are shown in Table 1. The following conditions will be assumed: 1) the mathematical model of the undamaged

system, i.e., the mass and stiffness distribution, are known and have been verified by test data; 2) the mass distribution and geometric configuration of the damaged system remain unchanged; and 3) the natural frequencies and mode shapes of the damaged system are measured; they may be incomplete in the sense that not all of the modes are measured.

With these data and these assumptions, the questions of detecting the occurrence of damage and its location and quantifying its the extent will be addressed. First, a comparison of the frequencies and mode shapes of the undamaged and damaged system will be made.

Let

$$\delta_i = \frac{(\omega_i)_{\text{undamaged}} - (\omega_i)_{\text{damaged}}}{(\omega_i)_{\text{undamaged}}} \tag{32}$$

$$\epsilon_i = \left\{ \sum_{j=1}^{j=3} [(x_j)_{\text{undamaged}} - (x_j)_{\text{damaged}}]^2 \right\}^{1/2} \tag{33}$$

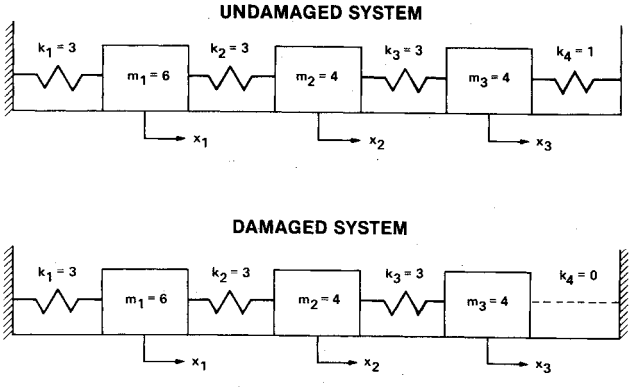

Fig. 1 Illustrative example.

Table 1 Eigenvalues and eigenvectors

	Undamaged			Damaged		
Mode	1	2	3	1	2	3
Frequency	0.500	1.000	1.500	0.375	0.953	1.483
Mode shape						
X_1	2.000	1.000	2.000	2.184	1.101	2.312
X_2	3.000	0	−5.000	3.756	0.200	−5.549
X_3	3.000	−1.000	3.000	4.624	−0.944	2.870

Table 2 Comparisons of frequency and mode shape

Mode	1	2	3
Frequency δ,%	25.000	4.700	1.130
Mode shape	0.271	0.232	0.083

Table 3 Kinetic energy distributions, %

Mode	1		2		3	
DOF	Undamaged	Damaged	Undamaged	Damaged	Undamaged	Damaged
X_1	25.00	16.77	60.00	66.15	15.00	17.07
X_2	37.50	32.98	0	1.47	62.50	65.45
X_3	37.50	50.16	40.00	32.39	22.50	17.49

Equation (32) is the percentage difference of the natural frequency, and Eq. (33) is the root-sum-square of the differences in the mode shapes. Because of the arbitrary normalization of the mode shapes, the maximum modal displacement in each mode is taken as unity in Eq. (33). Table 2 lists the comparisons of the frequencies and mode shapes. It is obvious that substantial changes exist for the first mode. This indicates that the structural system has changed, and since the mass distribution for this type of damage remains the same, it must be the stiffness that has changed. The location of the stiffness change will now be studied. Using Eq. (6), the kinetic energy distribution for the undamaged and damaged system have been calculated and are shown in Table 3. The kinetic energy distribution for each mode is listed in percentages for both the undamaged and damaged systems. The comparison indicates that the biggest difference between the two system always occurs at the degree-of-freedom x_3. It is reasonable to postulate that the damaged element is associated or physically attached to x_3. There are two structural elements associated with the x_3 degree of freedom, namely, the k_3 and k_4 springs. The k_3 spring is also associated with the x_2 degree of freedom whose kinetic energy remains relatively unchanged between the undamaged and damaged systems for all three modes. This implies that the corresponding strain energy distribution in the elements associated with x_2 degree of freedom, i.e., the springs k_2 and k_3, is relatively unchanged. Therefore, the only element whose strain energy must be changed to accommodate the kinetic energy distribution change is the k_4 spring. This concludes that the damage location is at the spring k_4.

Next, the damage of the structural member will be quantified by the procedure previously outlined. The stiffness matrix will be decomposed as indicated by Eq. (7) where $[K_0]$ is expressed by Eq. (31), and $[\Delta K]$ is defined as

$$[\Delta K] = \begin{bmatrix} \Delta k_1 + \Delta k_2 & -\Delta k_2 & 0 \\ -\Delta k_2 & \Delta k_2 + \Delta k_3 & -\Delta k_3 \\ 0 & -\Delta k_3 & \Delta k_3 + \Delta k_4 \end{bmatrix} \tag{34}$$

Now, let the ith mode shape vector $\{\phi\}_i$ be expressed as

$$\{\phi\}_i = \begin{Bmatrix} a_i \\ b_i \\ c_i \end{Bmatrix} \tag{35}$$

Equation (8) can then be written as

$$\begin{bmatrix} \Delta k_1 + \Delta k_2 & -\Delta k_2 & 0 \\ -\Delta k_2 & \Delta k_2 + \Delta k_3 & -\Delta k_3 \\ 0 & -\Delta k_3 & \Delta k_3 + \Delta k_4 \end{bmatrix} \begin{Bmatrix} a_i \\ b_i \\ c_i \end{Bmatrix} = \{y\}_i \tag{36}$$

where

$$\{y\}_i = \left(\omega_i^2 \begin{bmatrix} 6 & 0 & 0 \\ 0 & 4 & 0 \\ 0 & 0 & 4 \end{bmatrix} - \begin{bmatrix} 6 & -3 & 0 \\ -3 & 6 & -3 \\ 0 & -3 & 4 \end{bmatrix} \right) \begin{Bmatrix} a_i \\ b_i \\ \epsilon_i \end{Bmatrix} \tag{37}$$

From the left-hand side of Eq. (36), the connectivity matrix $[C]_i$ can be established as

$$[C]_i = \begin{bmatrix} a_i & a_i - b_i & 0 & 0 \\ 0 & b_i - a_i & b_i - c_i & 0 \\ 0 & 0 & c_i - b_i & c_i \end{bmatrix} \tag{38}$$

$$[C]_i \{\Delta k_{ij}\} = \{y\}_i \tag{39}$$

where

$$\{\Delta k_{ij}\} = \begin{Bmatrix} \Delta k_1 \\ \Delta k_2 \\ \Delta k_3 \\ \Delta k_4 \end{Bmatrix} \tag{40}$$

Equation (39) is the governing equation for solving for the various Δk_j. It has four unknowns, namely, Δk_1, Δk_2, Δk_3, and Δk_4, with three equations from each of the three degrees of freedom for each mode. Therefore, the solution procedure to be followed should be the one described by Eq. (21). Using the modal data listed in Table 1, one mode at a time, and Eq. (21), the solution for the Δk_j can be estimated. The results are listed in Table 4 in which the following definition should be noted:

$$\text{Stiffness reduction (\%)} = [\Delta k_j/(\Delta k_0)_j](\%) \tag{41}$$

From the mode 1 results, the stiffness reductions for spring k_1 to k_3 are from 1.56 to 4.22%. However, for spring k_4, the stiffness reduction is 97.69%. It is obvious that the spring k_4 has suffered major damage, and in view of the large stiffness reduction, one may conclude that the spring has been broken. Mode 1 test data correctly assesses the damage. As expected, mode 2 and 3 test data provide somewhat ambiguous results because of the small differences between the data from the damaged and the undamaged systems. Although the spring k_4 is identified to be damaged by a 71.46 or 64.06% stiffness reduction, these numbers are not convincing enough to indi-

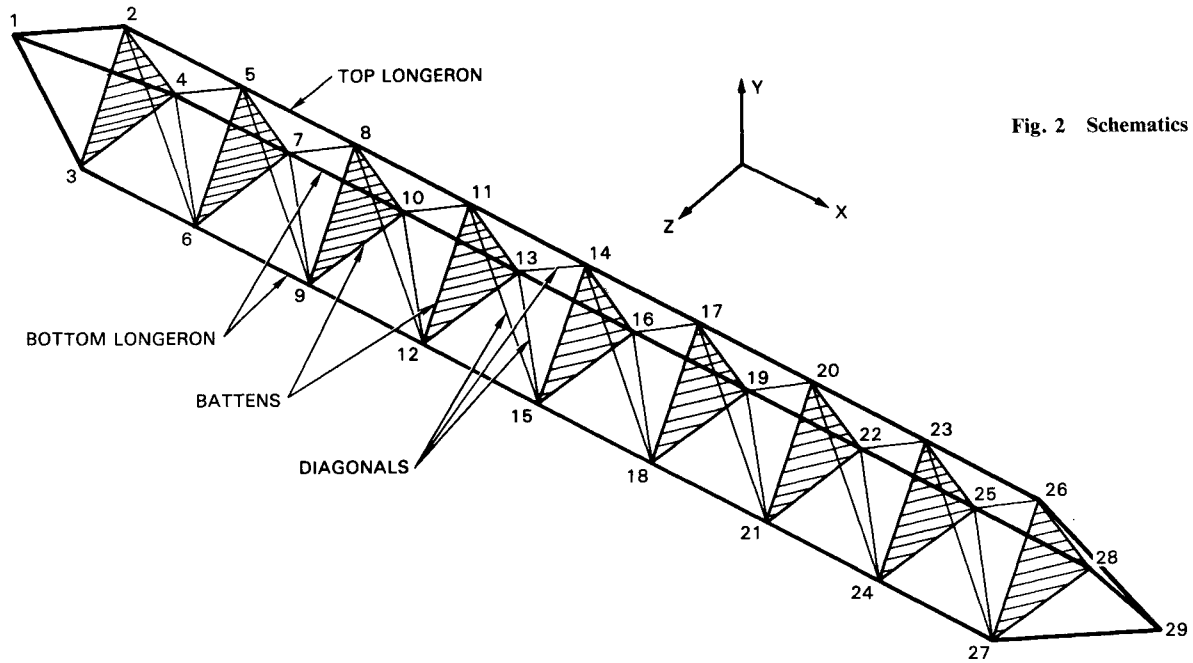

Fig. 2 Schematics of MAST truss.

Table 4 Damage assessment for each mode

Mode	1		2		3	
Element	ΔK_j	Stiffness reduction, %	ΔK_j	Stiffness reduction, %	ΔK_j	Stiffness reduction, %
K_1	−0.0468	1.56	0.2391	−7.97 (increased)	−0.4440	14.8
K_2	−0.0694	2.31	−0.2992	9.97	0.1293	−4.31
K_3	−0.1265	4.22	−0.2378	7.93	−0.1236	4.12
K_4	−0.9769	97.69	−0.7146	71.46	−0.6406	64.06

Table 5 Damage assessment for multiple modes

Mode	1 and 2		2 and 3		3 and 1		1, 2, and 3	
Element	ΔK_j	Stiffness reduction, %	ΔK_j	Stiffness reduction, %	ΔK_j	Stiffness reduction, %	ΔK_j	Stiffness reduction, %
K_1	−0.0003	0.01	−0.0038	0.13	0.0018	−0.06 (increased)	0.0010	0.03 (increased)
K_2	−0.0039	0.13	−0.0003	0.01	−0.0019	0.06	−0.0017	0.06
K_3	−0.0049	0.16	−0.0025	0.08	−0.0011	0.04	−0.0012	0.04
K_4	−0.9996	99.96	−0.9961	99.61	−1.0000	100	−1.0000	100

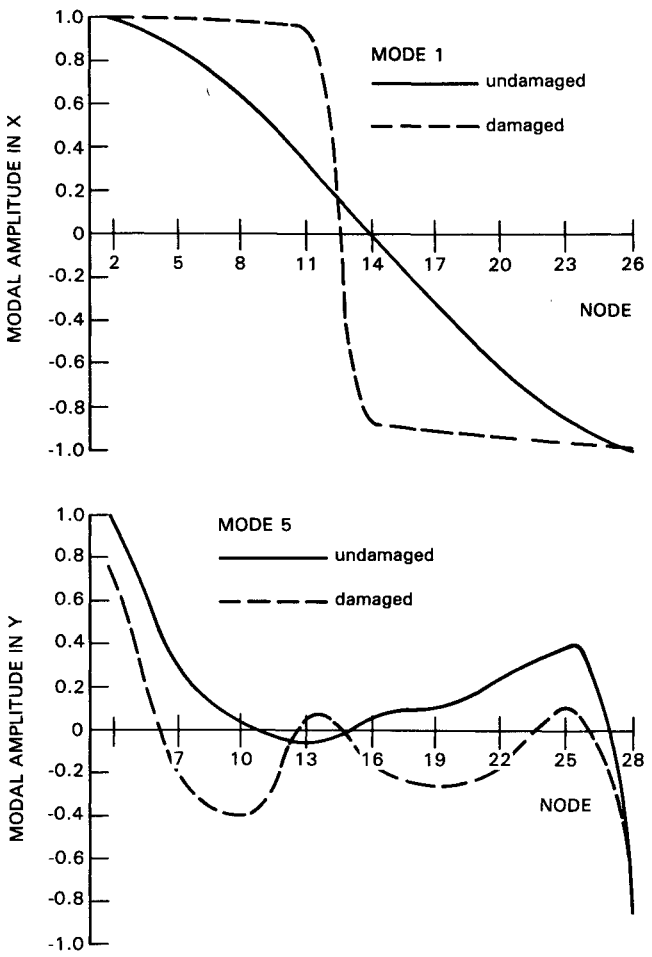

Fig. 3 Modal amplitude comparison.

Table 6 Dimensions and material properties

Element	Elastic modulus E, N/m^2	Area A, cm^2	Poisson's ratio ν	Material[a] density, kg/m^3
Top longerons	66.33×10^9	1.8097	0.3	2.1704×10^3
Bottom longerons	66.33×10^9	1.4142	0.3	2.1704×10^3
Diagonals	66.33×10^9	0.4185	0.3	4.4399×10^3
Battens	66.33×10^9	0.2271	0.3	1.6481×10^3
Damaged[b] longerons	6.895×10^3	1.8097	0.3	2.1704×10^3
Damaged[c] longeron	6.895×10^3	1.4142	0.3	2.1704×10^3

[a]Concentrated mass of 0.357 kg is added to each node representing the joint mass. [b]Element between nodes 11 and 14. [c]Element between nodes 21 and 24.

cate a breakage. However, these numbers should be sufficient to indicate that a damage has occurred at the spring k_4.

For multiple measured modes, Eq. (12) will be used, and the solution procedure is the one expressed by Eq. (25). The results are listed in Table 5. It is clearly demonstrated that the proposed approach works perfectly in this case. The k_4 spring is identified as having 100% stiffness reduction, which is total breakage, and the springs k_1, k_2, and k_4 are identified as having less than 1% of stiffness changes. It is interesting to note that when mode 2 and 3 data were used separately, it provided less accurate assessment, but when combined, a very accurate assessment is obtained.

Table 7 System modal data

Undamaged case			
Mode number	Frequency, Hz	Effective mass, %	
		X DOF	Y DOF
1	0.884861	0.000	85.165
2	2.462949	0.007	0.000
3	4.005897	0.000	7.404
4	5.290891	0.046	0.000
5	5.985745	90.855	0.000
6	6.545278	0.000	2.596
7	7.039045	0.184	0.000
8	8.226030	0.041	0.000
9	8.231417	0.000	0.262
10	9.171545	0.076	0.000

Damaged case			
Mode number	Frequency, Hz	Effective mass, %	
		X DOF	Y DOF
1	0.459477	0.029	83.105
2	2.300969	0.184	0.266
3	3.870547	0.061	8.790
4	5.181898	0.066	0.026
5	5.656655	85.241	0.076
6	6.096672	0.946	1.176
7	6.962743	0.564	0.218
8	7.780087	0.002	0.962
9	8.136252	0.593	0.087
10	8.657618	0.008	1.650

Table 8 Mode shape (1) comparison

Node	Undamaged case		Damaged case	
	X DOF	Y DOF	X DOF	Y DOF
2	−1.000	0.223	−1.000	0.230
3	−0.523	0.216	−0.402	0.216
4	−0.587	0.263	−0.403	0.226
5	0.851	0.526	0.999	0.466
6	−0.493	0.482	−0.363	0.457
7	−0.468	0.577	−0.341	0.477
8	0.617	0.777	0.980	0.696
9	−0.400	0.744	−0.310	0.686
10	−0.308	0.817	−0.273	0.704
11	0.325	0.939	0.948	0.903
12	−0.253	0.924	−0.244	0.897
13	−0.122	0.963	−0.203	0.964
14	0.000	0.995	−0.867	0.943
15	−0.072	1.000	−0.167	1.000
16	0.072	1.000	−0.086	0.945
17	−0.325	0.939	−0.903	0.816
18	0.122	0.963	−0.134	0.823
19	0.253	0.924	0.035	0.816
20	−0.618	0.777	−0.930	0.662
21	0.308	0.817	−0.109	0.676
22	0.400	0.744	0.169	0.646
23	−0.851	0.526	−0.953	0.447
24	0.468	0.577	0.402	0.451
25	0.493	0.482	0.262	0.432
26	−1.000	0.223	−0.956	0.220
27	0.587	0.263	0.423	0.219
28	0.523	0.216	0.324	0.196

Next, a MAST beam will be used as an example. Figure 2 shows the schematic of the space beam with the node numbers for the finite-element analysis. For the damaged structure, the elastic modulus of two of the longerons are reduced almost to zero. Table 6 shows the dimensions and the material properties of the space beam. Table 7 shows the modal analysis results for the undamaged and damaged systems. For the first 10 modes, only the first mode shows substantial change in

Table 9 Mode shape (5) comparison

	Undamaged case		Damaged case	
Node	*X* DOF	*Y* DOF	*X* DOF	*Y* DOF
2	0.578	−0.876	0.352	−0.368
3	0.454	0.828	0.409	1.000
4	0.521	1.000	0.408	0.737
5	0.766	0.056	0.458	−0.017
6	0.651	−0.386	0.561	0.057
7	0.731	0.287	0.584	−0.198
8	0.897	−0.034	0.561	−0.256
9	0.805	0.065	0.697	0.071
10	0.879	0.038	0.717	−0.398
11	0.975	−0.129	0.599	−0.032
12	0.916	−0.107	0.819	0.180
13	0.962	−0.055	0.792	0.048
14	1.000	0.000	0.853	−0.017
15	0.972	−0.086	0.910	0.399
16	0.972	0.086	0.803	−0.156
17	0.975	0.129	0.801	−0.234
18	0.962	0.055	0.970	−0.044
19	0.916	0.107	0.752	−0.274
20	0.897	0.035	0.702	−0.015
21	0.879	−0.038	1.000	0.124
22	0.805	−0.065	0.623	−0.191
23	0.766	−0.056	0.578	−0.192
24	0.731	−0.287	0.322	−0.698
25	0.651	0.386	0.492	0.113
26	0.578	0.875	0.430	0.607
27	0.521	−1.000	0.263	−0.600
28	0.455	−0.829	0.342	−0.575

Table 10 Kinetic energy change ratios

	Mode 1		Mode 5	
Node	*X* DOF	*Y* DOF	*X* DOF	*Y* DOF
2	0.793+0	0.270+0	−0.442+0	−0.701+0
3	0.618−1	0.191+0	0.214+0	0.146+1
4	−1.155+0	−0.166+0	−0.783−1	−0.804−1
5	0.147+1	−0.639−1	−0.399+0	−0.851+0
6	−0.271−1	0.704−1	0.112+0	−0.963+0
7	−0.502−1	−0.185+0	−0.418−1	−0.196+0
8	0.351+1	−0.449−1	−0.413+0	0.924+2
9	0.816−1	0.135−1	0.124+0	0.100+1
10	0.406+0	−0.115+0	−0.311−2	0.187+3
11	0.142+2	0.989−1	−0.434+0	−0.896+0
12	0.664+0	0.121+0	0.201+0	0.378+1
13	0.397+1	0.192+0	0.168−1	0.272+0
14	1.377+9	0.680−1	0.921−1	0.140+8
15	0.856+1	0.189+0	0.314+0	0.357+2
16	0.150+1	0.616−1	0.243−1	0.464+1
17	0.128+2	−0.101+0	0.136−1	0.454+1
18	0.116+1	−0.131+0	0.524+0	0.960−1
19	−0.965+0	−0.727−1	0.120−1	0.100+2
20	0.306+1	−0.135+0	−0.808−1	−0.668+0
21	−0.777+0	−0.185+0	0.940+0	0.174+2
22	−0.680+0	−0.101+0	−0.100+0	0.136+2
23	0.124+1	−0.141+0	−0.147+0	0.191+2
24	0.322+0	−0.273+0	−0.708+0	0.900+1
25	−0.493+0	−0.444−1	−0.141+0	−0.855+0
26	0.640+0	0.158+0	−0.170+0	−0.187+0
27	−0.677−1	−0.173+0	−0.617+0	−0.390+0
28	−0.309+0	−0.128−1	−0.151+0	−0.184+0

frequency, which indicates that something has happened. Based on an evaluation of the effective mass, only mode 1 and mode 5 are of global nature, and the other modes are local modes because of the small effective mass. The mode shapes of these two global modes are compared in Tables 8 and 9 for mode 1 and mode 5, respectively. The applitudes of the modal displacements are normalized such that the maximum amplitude is unity in the x or y-direction. The normalization is

Table 11 Estimated stiffness changes, $\Delta k_{ij}/k_{ij}$

	DOF			DOF	
No.	*i,j*		No.	*i,j*	
1	1, 1	0.257−1	40	27,27	−0.117−1
2	1, 7	0.434−1	41	27,33	−0.893−1
3	2, 2	−0.947−6	42	28,28	0.786−9
4	3, 3	−0.520−3	43	29,29	0.310−7
5	3, 9	−0.946−3	44	29,35	−0.605−7
6	4, 4	0.149−6	45	30,30	−0.156−6
7	5, 5	0.138−6	46	31,31	0.956−1
8	5,11	0.110−5	47	31,37	(−0.134+0)
9	6, 6	−0.304−5	48	32,32	−0.441−6
10	7, 7	−0.403−1	49	33,33	0.399−1
11	7,13	(−0.132+0)[a]	50	33,39	0.245+0
12	8, 8	−0.938−6	51	34,34	−0.325−8
13	9, 9	0.704−3	52	35,35	−0.165−7
14	9,15	0.304−2	53	35,41	0.508−7
15	10,10	−0.883−6	54	36,36	−0.138−6
16	11,11	−0.505−6	55	37,37	−0.369−1
17	11,17	−0.127−5	56	37,43	0.498−1
18	12,12	−0.686−7	57	38,38	0.372−7
19	13,13	0.993−1	58	39,39	(−0.117+0)
20	13,19	0.360+0[b]	59	39,45	(−0.111+1)
21	14,14	−0.171−5	60	40,40	0.158−6
22	15,15	−0.169−2	61	41,41	0.269−6
23	15,21	−0.926−2	62	41,47	−0.274−5
24	16,16	−0.273−6	63	42,42	−0.141−6
25	17,17	0.786−6	64	43,43	0.150−1
26	17,23	0.631−6	65	43,49	−0.162−1
27	18,18	−0.475−7	66	44,44	−0.187−7
28	19,19	(−0.255+0)	67	45,45	(−0.277+0)
29	19,25	(−0.108+1)	68	45,51	0.338+0
30	20,20	0.130−6	69	46,46	0.295−6
31	21,21	0.435−2	70	47,47	0.128−5
32	21,27	0.311−1	71	47,53	−0.156−5
33	22,22	−0.192−6	72	48,48	0.868−6
34	23,23	−0.647−6	73	49,49	−0.962−2
35	23,29	0.440−6	74	50,50	0.111−5
36	24,24	0.147−8	75	51,51	0.174+0
37	25,25	(−0.248+0)	76	52,52	−0.151−5
38	25,31	0.358+0	77	53,53	−0.145−5
39	26,26	0.412−6	78	54,54	0.155−6

[a]Possible damages.
[b]Increase stiffness not allowed, constrained in next iteration.

performed separately for the x and y displacements. Comparison of the damaged and undamaged shapes for mode 1 indicates that the displacements in the y-direction are very similar; however, substantial differences exist for the displacement in x-direction. It should be noted that mode 1 is predominantly a y-direction mode such that the modal displacements in y-direction are orders of magnitude greater than those of the x-direction. Yet, the differences are concentrated in the small-amplitude x-direction displacements. For mode 5, exactly the opposite is found. Figure 3 shows graphically the mode shape comparison for some of the degrees of freedom along the longerons. In spite of the substantial differences in frequency, mode shapes, and effective masses, the location of the damage cannot be definitively pinpointed. Next, the kinetic energy distribution will be examined. But first, the kinetic energy (KE) change ratio will be difined as

$$\text{Kinetic Energy Change Ratio} = \frac{(\text{KE})_{\text{undamaged}} - (\text{KE})_{\text{damaged}}}{(\text{KE})_{\text{undamaged}}} \tag{42}$$

Table 10 shows the kinetic energy change ratio for mode 1 and mode 5. At node 14, the kinetic energy change ratios are several orders of magnitude greater than at the rest of the nodes. This indicates that elements connected to node 14 may be damaged. However, no noticeable changes in kinetic energy

Table 12 Iterations of estimated stiffness changes

DOF		No. of iterations			
No.	*i,j*	First	Second	Third	Exact solution
1	1, 1	0.257−1	−0.183−5	−0.183−5	−0.387−4
3	2, 2	−0.947−6	−0.947−6	−0.947−6	−0.668−5
11	7,13	−0.132+0	−0.257−5	−0.257−5	−0.491−5
15	10,10	−0.883−6	−0.883−6	−0.883−6	0.000+0
20	13,19	0.360+0[a]	0.000+0[c]	0.000+0[c]	0.491−5
28	19,19	−0.255+0	−0.323+0	−0.465+0	−0.465+0[c]
29	19,25	−0.108+1[b]	−0.133+1[b]	−0.100+1[d]	−0.100+1[e]
37	25,25	−0.248+0	−0.296+0	−0.465+0	−0.465+0[c]
38	25,31	0.358+0[a]	−0.000+0[c]	0.000+0[c]	0.495−5
46	31,31	0.956−1	−0.493−7	−0.493−7	0.760−5
47	31,37	−0.134+0	0.655−6	0.655−6	0.491−5
50	33,39	0.245+0[a]	0.000+0[c]	0.000+0[c]	0.628−5
58	39,39	−0.117+0	−0.116+0	−0.454+0	−0.454+0[c]
59	39,45	−0.111+1[b]	−0.120+1[b]	−0.100+1[d]	−0.100+1[e]
67	45,45	−0.277+0	−0.429+0	−0.454+0	−0.454+0
68	45,51	0.338+0[a]	0.000+0[c]	0.000+0[c]	0.000+0
75	51,51	0.174+0[a]	−0.736−6	−0.736−6	0.337−5

[a]Increasing stiffness not allowed.
[b]Stiffness reduction more than 100%, not allowed.
[c]Constrained to zero increment.
[d]Constrained to 100% stiffness reduction.
[e]Significant stiffness reduction for the damages.

are shown at either node 21 or node 24 where the second damaged element is located.

Next, the damage of the structural member will be quantified by the procedure outlined previously. Only the modal data of the first mode will be used, which implies that the number of equations is equal to the number of degrees of freedom in Eqs. (8) or (10). The number of unknowns, namely, the elements in the $[\Delta K]$ matrix, consist of the diagonal elements and the banded off-diagonal terms. Therefore, there are more unknowns than equations, and the minimization procedure outlined in Case 1 will be applied. The resulting stiffness perturbation $\Delta \boldsymbol{k}_{ij}$ is listed in ratios of the estimated values and the corresponding undamaged quantities, as shown in Table 11. It is important that the following points be noted when the results are examined. First, it is assumed that damage occurs by breakage, i.e., reduction in stiffness; therefore, an increase in the stiffness is not allowed. Second, because of the numerical roundoff errors, any estimated stiffness change that is less than 10% of the undamaged value will be ignored. For instance, no. 20, the element $\Delta k_{13,19}$ is 0.36, which according to the model is the stiffness between nodes 8 and 11 in x-direction, and increment of 36% is certainly inconsistent with the expected results. Similar results are found in no. 38 $\Delta k_{25,31}$; no. 50 $\Delta k_{33,39}$; no. 68 $\Delta k_{45,51}$; and no. 75 $\Delta k_{51,51}$. These elements will be constrained in the next iteration of estimation in such a way that no positive increment is allowed. The exception is the $\Delta k_{51,51}$, since the 17.4% increase is considered small. Two other elements, no. 29 $\Delta k_{19,25}$ and no. 59 $\Delta k_{39,45}$, show a stiffness reduction of more than 100%, which is again physically impossible. However, since the values are not too much greater than 100%, they will not be constrained in the second iteration.

Table 12 lists the results from subsequent iterations for selected $\Delta \boldsymbol{k}_{ij}$. The stiffness reductions for $\Delta k_{19,25}$ and $\Delta k_{39,45}$ are greater than those of the first iteration. Therefore, they will be constrained to a value of 100% for the next iteration. For $\Delta k_{51,51}$, the stiffness increase becomes negligible. The only significant stiffness reductions are limited to $\Delta k_{19,19}$; $\Delta k_{19,25}$; $\Delta k_{25,25}$; $\Delta k_{39,39}$; $\Delta k_{39,45}$; and $\Delta k_{45,45}$. According to the finite-element model, degrees-of-freedom (19,25) and (39,45) are associated with nodes 11, 14 and 21, 24 in x-direction, respectively. The reductions of these elements in the stiffness matrix clearly indicates that the structural elements between these nodes have been severely damaged. The exact solution is also listed in the last column of Table 12, and a comparison indicates that the results from the third iteration are very accurate except for those values that are insignificantly small.

The damages to the structural system for the sample problem have been identified and the extent of the damage quantified. In fact, the results are very encouraging.

Concluding Remarks

Although the feasibility of using the proposed procedure for onboard structural damage assessment based on the measured modal data has been demonstrated by the example problem, many related issues have not yet been addressed. The questions regarding the accuracy requirement of the measurement, the completeness of the measurement with respect to the number of degrees of freedom in the analytical model, and the selection of which modal data to use are just some of these issues that are of critical importance for the actual application of the methodology. Furthermore, laboratory experiments should be performed to verify the procedure as part of the process to make the proposed methodology reach maturity.

Acknowledgment

The research was carried out by the Jet Propulsion Laboratory, California Institute of Technology, under a contract with NASA. This task was sponsored by Samuel L. Venneri, NASA Office of Aeronautics and Space Technology, Code RM.

References

[1]Vandiver, J. K., "Detection of Structural Failure on Fixed Platforms by Measurement of Dynamic Response," *Proceedings of the Offshore Technology Conference,* Vol. 2, Paper OTC 2267, May 1975, pp. 243–252.

[2]Wojnarowski, M. E., Stiansen, S. G., and Reddy, N. E., "Structural Integrity Evaluation of a Fixed Platform Using Vibration Criteria," *Proceedings of the Offshore Technology Conference,* Vol. 3, Paper OTC 2909, May 1977, pp. 247–256.

[3]Coppolino, R. N. and Rubin, S., "Detectability of Structural Failures in Offshore Platforms by Ambient Vibration Monitoring," *Proceedings of the Offshore Technology Conference,* Vol. 1, Paper OTC 3865, May 1980, pp. 101–110.

[4]Thoren, A. R., "Derivation of Mass and Stiffness Matrices from Dynamic Test Data," AIAA Paper 72-346, April 1972.

[5]Berman, A. and Flannelly, W. G., "Theory of Incomplete Models of Dynamics Structures," *AIAA Journal,* Vol. 9, Aug. 1971, pp. 1481–1487.

[6]Chen, J. C. and Garba, J. A., "Analytical Model Improvement Using Modal Test Results," *AIAA Journal,* Vol. 18, June 1980, pp. 684–690.

[7]Chen, J. C., Peretti, L. F., and Barba, J. A., "Spacecraft Structural System Identification by Modal Test," *Journal of Spacecraft and Rockets,* Vol. 24, Jan.–Feb. 1987, pp. 90–94.

[8]Chen, J. C., "Analytical Model Accuracy Requirements for Structural Dynamic Systems," *Journal of Spacecraft and Rockets,* Vol. 21, July–Aug. 1984, pp. 366–373.